

Towards a Simple, Fast, Oscillation-free, High-resolution Algorithm for Convection-Dominated Flows: The Position-State Separation Method

Lipeng Liu¹, Marley Becerra¹

¹Royal Institute of Technology –KTH–, School of Electrical Engineering, Stockholm, 100 44, Sweden

Corresponding author's e-mail: lipeng@kth.se

Abstract— A simple, fast, oscillation-free, high-resolution algorithm for convection-dominated flows is proposed. The stability, accuracy and time complexity of this method called the position-state separation method (POSS) are discussed. Several classical numerical experiments in different dimensions and coordinate systems are conducted to demonstrate the excellent performance of the POSS regarding computational cost, robustness, and high-resolution. It is shown that the step time of POSS is not restricted by the Courant–Friedrichs–Lewy condition and that the time complexity of the method when dealing with the convection-dominated flows increases linearly with the number of unknowns.

Contents

1	Introduction.....	3
2	The Position-State Separation Method.....	5
3	Numerical Implementation	8
3.1	Mesh generation	9
3.2	Solution of the state and position subproblems.....	10
3.3	Projection and boundary condition.....	11
4	Features of the method.....	13
4.1	Stability.....	13
4.2	Accuracy	13
4.3	Time complexity	15
4.4	Extension to other coordinate systems.....	15
5	Numerical experiments	16
5.1	Rotation of a Cylinder with a slot.....	16
5.2	General advection-diffusion problem test.....	17
5.3	Davies test	18
5.3.1	1D Davies test.....	18

5.3.2 2D Davies test..... 20

5.3.3 3D Davies test..... 22

5.4 2D streamer discharge test 23

6 Conclusion 25

Acknowledgments..... 25

References..... 25

1 Introduction

The convection–diffusion–reaction (CDR) equation is a mathematical model often used to evaluate the variation of a physical quantity u in a flow under the influence of processes of convective bulk movement, diffusive motion and interconversion with other quantities. It is widely used in electrodynamics, chemistry, population biology and plasma physics as an equation given by

$$\frac{\partial u}{\partial t} + \nabla \cdot (\mathbf{v}u - D\nabla u) = f \quad (1.1)$$

where \mathbf{v} is the velocity vector of the flow and D is the diffusion coefficient. The term f defines the sources and sinks due to interconversion (reaction) processes. In general, this equation is difficult to solve numerically in cases where u or \mathbf{v} exhibits shocks, discontinuities or steep gradients, especially when the flow is convection-dominated. For this reason, numerous numerical methods have been developed over the last four decades. However, all of them have suffered from drawbacks such as artificial oscillation, excessive numerical diffusion or heavy demand for computation time and resources.

Generally, the numerical methods for convection-dominated problems can be divided from the perspective of the frame of reference into three groups: Eulerian, Lagrangian and mixed Eulerian-Lagrangian. Let us now briefly describe the main features of the most common methods for solving CDR equations in plasma physics. For a detailed discussion of the subject, the reader is referred to [1, 2].

For most Eulerian methods, the ‘flux limiting’ concept is generally used to avoid spurious oscillations occurring at discontinuities and shock fronts when high order spatial discretization schemes are used. One of the first methods to introduce this concept was the flux-corrected transport method (FCT) [3-5]. Since the FCT was originally proposed by Boris and Book for uniform meshes in one dimension, its extension to high dimensions and non-uniform mesh was later suggested by Zalesak [6] and Morrow [7], respectively. Shortly afterwards, the finite-element FCT method (FEM-FCT) was presented to handle irregular structures [8, 9]. FEM-FCT is based on Zalesak’s FCT procedure dealing with element contributions, which was later modified by introducing the bilateral mass exchange between individual nodes [10]. However, Zalesak’s ‘flux limiting’ is time consuming. Following the concept of ‘flux limiting’,

other high-resolution algorithms such as MUSCL (monotone upstream-centered schemes for conservation laws) scheme [11], QUICK (quadratic upstream interpolation for convective kinetics) scheme [12] and TVB-DG (total-variation-bounded discontinuous Galerkin finite element method) [13-17] were also proposed. All of them can be viewed as different combinations of the finite element method (FEM) or the finite volume method (FVM) with different flux or slope limiters. However, the major disadvantage of these Eulerian, high-resolution schemes is that they are restricted by the Courant–Friedrichs–Lewy condition (CFL condition) and need flux limitation, which is computationally expensive.

Purely Lagrangian methods are rarely used since severe problems occur when the discretization is performed on a moving Lagrangian mesh. Instead, mixed concepts that combine the advantages of Lagrangian and Eulerian methods are often used, which in essence follow the “exact-transport + projection” approach [18]. The basic idea is to use the Lagrangian method to calculate the exact transport of the unknown variables and then to project the obtained solution back onto an Eulerian mesh where the unknown variable is presented and other dependent variables are computed. This approach is essentially the same as the method of characteristics [19] whose idea is to discretize the total derivative $\frac{Du}{Dt}$ (also called material derivative) in time instead of $\frac{\partial u}{\partial t}$. It is worthy to mention that the method of characteristics is in fact a particles-in-cell (PIC) method [20]. Overall, the main weaknesses of the existing Lagrangian-Eulerian methods can be summarized as:

- the ‘projection’ procedure is either time or resource consuming such as the least-squares Galerkin method [20];
- most of the methods can only deal with incompressible flows, i.e. with the restriction $\nabla \cdot \mathbf{v} = 0$ [1, 2, 18, 20]; and
- the particle meshless method suffers from discrete particle noise such as the PIC method [21, 22].

To the authors' knowledge, none of the existing Lagrangian-Eulerian schemes is free from the above problems. Summarizing, an improved numerical method should be:

- able to provide accurate, stable and non-negative solutions in the presence of shock fronts, discontinuities or steep gradients. This means the solution should be neither diffusive nor heavily fluctuating and also have physical meaning;
- easy and fast, which means the algorithm is easy to implement and also computationally cheap;
- easily implemented on irregular region and unstructured mesh;
- extendable to high dimensions and other coordinate system; and
- feasible for parallel computation.

In this paper, a simple, fast, oscillation-free, high-resolution method for solving convection-dominated problems with reaction and diffusion terms is presented. The proposed approach, referred to as the position-state separation method (POSS), uses operator-splitting [23] to combine an Eulerian scheme for the solution of the convective acceleration, the diffusion and the reaction subproblem and a semi-Lagrangian scheme for the solution of the linear convection subproblem. The Eulerian solution is based on Galerkin finite element method [24]. The semi-Lagrangian subproblem is based on the solution in an auxiliary mesh where each individual node during the simulation follows the flow only during the current time step, instead of using a moving mesh or a particle meshless concept. Simple linear interpolation is used for the projection of the solution from the auxiliary mesh to the Eulerian mesh.

The paper is organized as follows. The basic concept, the numerical implementation and the features of the method are introduced in Section 2, 3 and 4, respectively. Section 5 is devoted to numerical experiments. Conclusions are drawn in the last section.

2 The Position-State Separation Method

The three essential elements of unsteady particle flow are time, position and state. Difficulties arise when the time discretization and space discretization of the same unknown variable are mixed in one equation. The basic idea of the POSS is to split the transient solution of the position and the state of the physical quantity u into two different numerical problems and to use the most suitable solution method for each.

For sake of simplicity, let us first consider the CDR problem in one dimension (1D) and assume the diffusion coefficient D is constant. Then, equation (1.1) is rewritten as

$$\frac{\partial u}{\partial t} + v \frac{\partial u}{\partial x} = D \frac{\partial^2 u}{\partial x^2} - u \frac{\partial v}{\partial x} + f \quad (2.1)$$

where $x \in [a, b]$, $a < b$ is the computation domain discretized in space with an Eulerian mesh with N nodes (hereinafter called reference mesh). By performing operator-splitting [23], equation (2.1) is divided into two different expressions such that its solution is approximated by the sequential solution of two separate subproblems:

a) the state subproblem given by

$$\frac{\partial u}{\partial t} = D \frac{\partial^2 u}{\partial x^2} - u \frac{\partial v}{\partial x} + f \quad (2.2)$$

which deals with the variation of the variable u due to diffusion, convective acceleration and the reaction terms. The solution of this equation provides the initial condition u^* to the second subproblem during each time step.

b) the position subproblem given by

$$\frac{\partial u}{\partial t} + v \frac{\partial u}{\partial x} = 0 \quad (2.3)$$

which determines the transport of the variable u by considering the linear convection only.

Since operator splitting is independent of the number of dimensions involved, this approach can be easily extended to two or three dimensions (2D/3D). Rewriting equation (2.2) and (2.3) in their multi-dimensional forms yields

$$\frac{\partial u}{\partial t} = D \Delta u - u \nabla \cdot \mathbf{v} + f \quad (2.4)$$

$$\frac{\partial u}{\partial t} + \mathbf{v} \cdot \nabla u = 0 \quad (2.5)$$

where the unknown variable u is defined in a space variable \mathbf{x} belonging to the bounded domain $\Omega \subset \mathfrak{R}^d$ ($d=1, 2, 3$), and a velocity vector \mathbf{v} .

The state subproblem (2.4) is simple to solve with any Eulerian scheme in a reference mesh since the discretization of space and time is performed for different variables (u and \mathbf{v} respectively). Thus, equation (2.4) can be computed using a variety of numerical methods such as FVM or FEM (used in this paper). In turn, the solution to the position subproblem (2.5) is a hard numerical problem in the presence of discontinuities or high gradients due to discretization difficulties if an Eulerian scheme is used. In this paper, a semi-Lagrangian scheme based on the method of characteristics is used to obtain the exact transport of the variable u by using as initial value the solution of the state problem u^* at each time step. Thus, equation (2.5) is solved by integrating the ordinary differential equation

$$\frac{\partial \mathbf{x}}{\partial t} = \mathbf{v} \quad (2.6)$$

along the characteristic lines of the flow. In contrast to the other Lagrangian or semi-Lagrangian methods, individual parcels of fluid are not followed through time with a moving mesh or a system of particles. Instead, individual parcels of fluid located at the nodes of the reference mesh (used for the state subproblem) are tracked along their characteristic paths only during each time step. Then, the displacement of these parcels of fluid defines the nodes of an auxiliary mesh which is created from the reference mesh. One advantage of this approach is that the auxiliary mesh does not become excessively distorted (as a Lagrangian moving mesh) since it only “flickers” (depending on the variations of the local velocity vectors) around the corresponding nodes in the reference mesh. For this reason, the method does not require any mesh adaptivity or reconstruction algorithm, which is a computationally expensive step especially in three dimensions. Compared with some particle meshless method such as the particle transport method (PTM) [1, 2] which needs ‘particle adaptivity’ during each time step, the auxiliary mesh used here is also much easier to implement.

Once the solution to the position subproblem defines the location of the auxiliary mesh, the transported state of the unknown variable is projected back to the reference mesh. The projection is done using linear interpolation. For a 1D mesh, the state at one positive is obtained by linear interpolation from the two adjacent points. For a 2D or 3D mesh, the projection from the auxiliary mesh to reference mesh is implemented by Delaunay triangulation and linear interpolation with the scattered points (i.e. the nodes of the auxiliary mesh).

In order to further illustrate how POSS works, let us consider the 1D CDR problem with constant velocity v , without diffusion and with a constant loss reaction term. Space is discretized with a reference mesh with the uniform spacing length Δx . Fig.2.1 shows the sequential solution to the state and position subproblems after a simulation time step Δt for an arbitrary profile of u at the time t_0 .

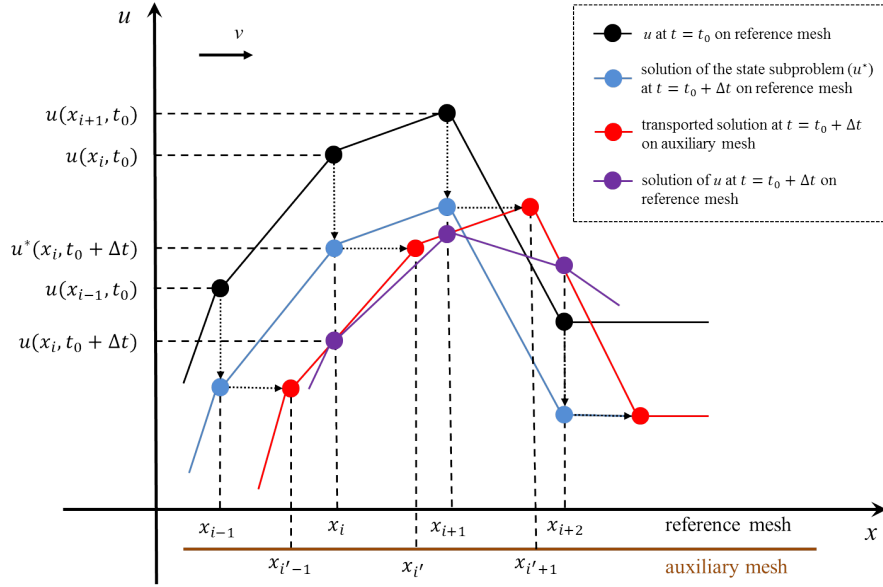


Fig.2.1. Illustration of the steps of the POSS to solve a 1D profile u during the time interval $[t_0, t_0 + \Delta t]$.

As it can be seen, the solution at each simulation time t consists of three main steps:

- i. the estimation of the magnitude (i.e. the state) of the unknown variable u in the reference mesh considering the convective acceleration as well as the diffusive and reaction terms;
- ii. the exact transport of the updated state u^* of the unknown variable such that the position of the solution is obtained in the auxiliary mesh; and
- iii. the projection of the solution obtained in the auxiliary mesh back to the reference mesh.

3 Numerical Implementation

Fig.3.1 shows the flow chart of the numerical implementation of POSS according to the approach presented in the previous section. The details of each block in the flow chart are discussed in the following sub-sections. The main idea of the algorithm is described as follows.

At first, the reference mesh is generated based on the computation region of the problem that is to be solved. The algorithm is continued step by step until the stop criterion is satisfied. During each simulation loop, there main steps are executed. First, the state subproblem (2.4) is solved on the reference mesh. Second, the auxiliary mesh is generated by solving the position subproblem (2.5). Third, the solution after each step is obtained by projection of the solution in the auxiliary mesh to the reference mesh. These steps are followed by the adjustment of the solution according to the boundary conditions of the problem. The choice of time step Δt will be discussed in Section 4 in details.

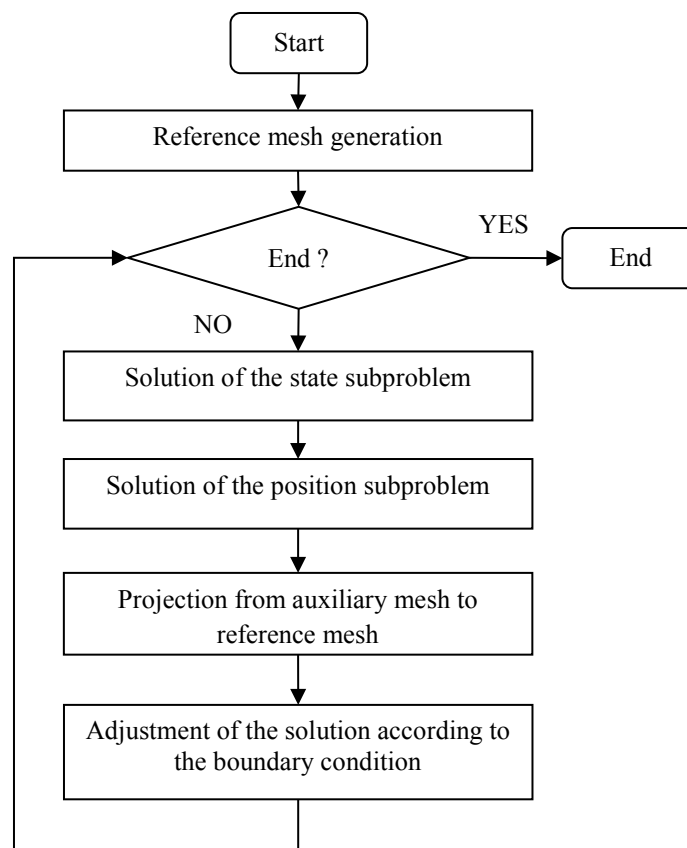


Fig.3.1. *The flow chart of POSS*

3.1 Mesh generation

The POSS does not have any restriction regarding the type of elements used for meshing the reference mesh. In this paper, the Delaunay triangulation algorithm is used with triangular and tetrahedrons mesh elements in 2D and 3D simulations, respectively. The reference mesh can be

unstructured where necessary. It is worth mentioning that the reference mesh can be ‘stationary’ throughout the calculations or it can be a ‘moving’ mesh when necessary as in the case of other adaptive moving-mesh Eulerian methods used to track the spatial variation of unknowns. In either case, the auxiliary mesh is updated at each time step from the location of the nodes in the corresponding reference mesh..

For the sake of simplicity, linear basis functions are chosen to represent the unknowns. In this way, some calculations for example the stiffness matrix and consistent mass matrix for solving equation (2.4) using FEM can be computed analytically.

3.2 Solution of the state and position subproblems

The solution of state subproblem on the reference mesh is here computed with the Galerkin finite element method [24]. If the diffusion term is present, equation (2.4) is always solved using the implicit schemes. Note that the boundary conditions have to be taken into account when solving the state subproblems (see [24] for more details).

Additionally, for convection-dominated flows when diffusion term could be neglected, the calculation of the divergence of the velocity field (due to convective acceleration) in equation (2.4) is vital. Since linear basis functions are used, the divergence of velocity at each element is constant. To obtain its value at each node, the divergence of velocity is computed using Galerkin FEM by

$$\mathbf{M}_c \nabla \cdot \mathbf{v} = \mathbf{f}_v \quad (3.1)$$

where \mathbf{M}_c is the global consistent matrix, $\nabla \cdot \mathbf{v}$ is the vector of velocity divergence and \mathbf{f}_v is the contribution vector assembled by the constant value of each element. Due to the linear basis function, the local consistent matrix is easy to be computed analytically. Note that element contribution calculation can be done using parallel computation and \mathbf{M}_c does not change for the reference mesh. Thus, equation (2.4) could be solved using the explicit method for convection-dominated flows. For 1D problem, when \mathbf{M}_c is usually not heavy, its inverse can be computed and stored at the beginning of the simulation. For 2D/3D problems, when the inverse of matrix \mathbf{M}_c is usually impossible to be stored, the incomplete Cholesky conjugate gradient (ICCG) method [25] is here used to solve equation (3.1).

As mentioned before, the position subproblem could be solved by integrating equation (2.6) along the characteristic lines of the flow. This is an ordinary differential equation which is easy to be solved. First-order Euler method is used for ordinary flows. And for the flows where velocity field changes dramatically over time and space, to obtain high-resolution, high order time discretization schemes have to be used to solve both the state and position subproblems.

For explicit time discretization schemes, high order TVD-RK (total variation diminishing Runge-Kutta method) is used [26]. For the ODE (ordinary differential equation) expressed as $u_t = L(u)$ the third order TVD-RK is given by

$$\begin{cases} u_1 = u^n + \Delta t L(u^n) \\ u_2 = \frac{3}{4} u^n + \frac{1}{4} [u_1 + \Delta t L(u_1)] \\ u^{n+1} = \frac{1}{3} u^n + \frac{2}{3} [u_2 + \Delta t L(u_2)] \end{cases} \quad (3.2)$$

Regarding equation (3.2), the value $L(u_1)$ and $L(u_2)$ above correspond to the velocities at two interval time steps. They are computed using linear interpolation from the initial position (x^n) to the interval position (x_1) and (x_2) during each time step.

In addition, if the diffusion term is neglected, the state subproblem could be viewed as an ODE which could be solved using TVD-RK. While for the cases with diffusion term, high order BDF (backward differential formula) combined with Galerkin FEM is used.

3.3 Projection and boundary condition

In order to describe more generally the projection step with POSS, a 2D computation region with inlet, outlet and wall is considered. To illustrate the computation region, several representative nodes are selected as example. Fig.3.2 shows an example of the reference mesh in two dimensions during one time step, together with the auxiliary mesh generated from it. For simplicity, the inlet and outlet are represented by a single blue and red solid circle, and named as ‘moving in nodes’ and ‘moving out nodes’, respectively. The wall is represented by the black solid circles and named as ‘still nodes’. The black solid circle in the middle of the region represents the interior wall boundary. At can be seen, the interior nodes as well as the nodes ‘moving out’ and those moving along the boundary are within the domain of the auxiliary mesh. For those nodes the projection is done by linear interpolation using the triangles of the auxiliary

mesh which contain them. In Section 4, it will be shown that the adjacent nodes of each node of the auxiliary mesh do not change as long as the stability of the time step is satisfied. It means that it is not necessary to do Delaunay triangulation again as long as the reference mesh is unchanged. The information of the Delaunay triangulation when the reference mesh is generated can be stored and used when the projection is done. For the projection of the ‘moving in nodes’ extrapolation must be used since they are not within the domain of the auxiliary mesh. The linear extrapolation method is based on the least-squares approximation of the gradient at the inlet boundary. Linear interpolation is performed sequentially at each mesh node in the reference mesh in order to guarantee always a positive solution after the projection is done. Since each value of the nodes is independent of others, parallel computation could be applied for the projection step.

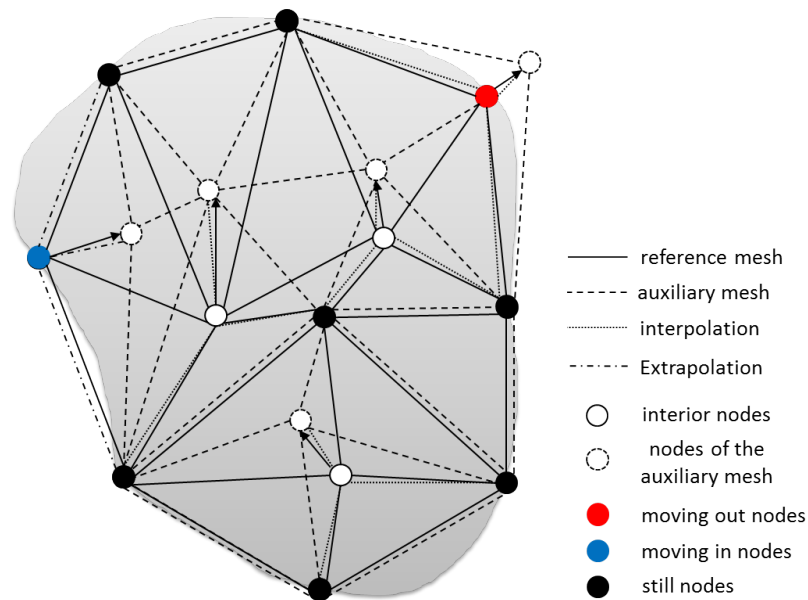


Fig.3.2. Example of a two-dimensional reference mesh and the auxiliary mesh generated according to the local velocity

Note that the error of linear interpolation (E_r) is proportional to the square of the distance between two nodes (Δx), i.e. $E_r \propto (\Delta x)^2$. Thus, a fine reference mesh could be easily used to reduce the error of the linear interpolation if needed.

After the projection, the unknowns on the boundaries are adjusted according to the boundary conditions of the equation to be solved. For the Dirichlet condition, the value of unknowns at the boundary is set directly. For the Neumann condition no further action is needed since it has already been taken into consideration in the solution of the state subproblem.

4 Features of the method

4.1 Stability

Let us take the case of one dimension as an example first. Since equation (2.3) is unconditionally stable, the only limitation comes from equation (2.2) if it is solved explicitly. In order to obtain a stable solution, it should be guaranteed that there is no inversion of any mesh element of the auxiliary mesh at any time. This means that the time step Δt possible at each time of the simulation is restricted by the following condition:

$$\Delta t < \min_{1 \leq i \leq N-1} \left(\frac{|\Delta x_{i,i+1}|}{|\Delta v_{i,i+1}|} \right) \quad (4.1)$$

where N denotes the total number of nodes, $\Delta x_{i,i+1}$ and $\Delta v_{i,i+1}$ are the space and velocity difference of the i^{th} and $(i+1)^{th}$ nodes, respectively. This condition has the concrete physical meaning that the time step should be chosen short enough to guarantee that no parcel of the fluid transported in the position subproblem can overrun others. In this case, the adjacent nodes of each node of the auxiliary mesh do not. The condition defines a maximum possible time step which is hereinafter referred to as the upper bound of stability Δt_{UBS} .

If we put this condition into equation (2.3), also expressed in the discretization form as $\frac{\Delta u}{\Delta t} = -u \frac{\Delta v}{\Delta x}$, the mathematic meaning will be derived: $\Delta u < -u$, which means that the decrement of the variable u due to convection during each step should not exceed its value. Thus, the variable u cannot become negative if condition (4.1) is satisfied, making the POSS method be positive preserving. Following this idea, in multi-dimensions, Δt_{UBS} can be expressed as:

$$\Delta t_{UBS}(t) = \min_{1 \leq i \leq N} \left(\frac{1}{|\nabla \cdot \mathbf{v}_i|} \right) \quad (4.2)$$

where $\nabla \cdot \mathbf{v}_i$ denotes the divergence of the velocity field. Note that Δt_{UBS} is only a necessary condition, not the sufficient condition to ensure stability.

4.2 Accuracy

The numerical accuracy of the POSS is mostly limited by the projection error, which is related to the simulation time step. In order to illustrate the projection error in the solution, let us

consider the 1D non-diffusive transport of a unitary square density pulse in a flow with constant velocity and free of source terms (i.e. a convection-dominated flow). As it can be seen in Fig.4.1, the obtained solution is as diffusive as the first order upwind difference method for very small time steps. It is easy to prove that POSS is exactly equivalent to upwind difference method with an extremely small time step. As the time step increases, the error in the projection step decreases. The physical interpretation of this is that the nodes should ‘run across’ the cells of the reference mesh which contain them, eliminating the diffusion effect caused by interpolation.

Thus, the minimum time step should be chosen to avoid excessive numerical diffusion in the solution such that the displacement of each node in the auxiliary mesh is larger than the corresponding space stepping Δx_i of the reference mesh. This condition defines that the time step Δt in the simulation should be larger than the lower bound of accuracy (LBA) of the step time Δt_{LBA} , defined as:

$$\Delta t_{LBA}(t) = \max_{1 \leq i \leq N} \left(\left| \frac{\Delta x_i}{v_i} \right| \right) \quad (4.3)$$

It is important to keep in mind that Δt_{LBA} is exactly the CFL condition. Additionally, in most cases, Δt_{UBS} will be much larger than Δt_{LBA} , which makes POSS extremely faster than other methods. If both UBS and LBA condition are satisfied, the error of POSS is mainly introduced by linear interpolation.

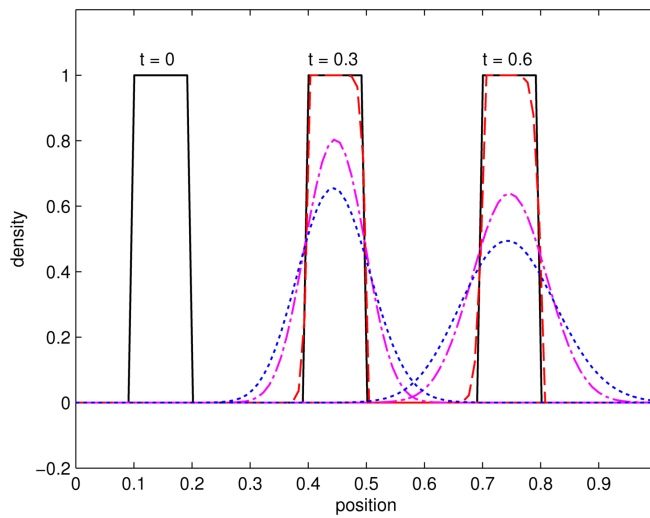


Fig.4.1. Results of a square test calculated with POSS with different time stepping: $\Delta t = 10^{-2}$ (dashed lines), $\Delta t = 5 \times 10^{-3}$ (dashdot lines) and $\Delta t = 5 \times 10^{-4}$ (dotted lines) for a 1D mesh with 100 cells. The exact solution is also plotted (solid lines).

It is important to point out that in some cases Δt_{UBS} can conflict with Δt_{LBA} . For example, the local values of $\frac{\Delta x_i}{v_i}$ of the low-velocity region can be very large, resulting in large Δt_{LBA} . In this situation, UBS condition has precedence over LBA condition to be satisfied. At this time, a certain degree of numerical diffusion will be introduced at low-velocity regions due to interpolation. However, the later numerical experiments will show that the introduced numerical diffusion will be rather small since in these places the u and v field are always non-stiff. For this reason, POSS could ensure high-resolution even though LBA condition is not satisfied.

Observe that the operator-splitting approach discussed in Section 2 introduces also an additional source of error to the estimates of POSS, which depends on the mesh, the step time and also the order of the schemes that used. Thus, it is difficult to generally quantify the splitting error for POSS. However, the numerical experiments in the following sections show that the splitting error could be considerably reduced as long as the UBS condition is satisfied and a high-order discretization scheme is used.

4.3 Time complexity

One of the most notable advantages of POSS is that it is computationally cheap. Observe that the computation time for Eulerian methods grow up exponentially with the number of cells. Moreover, smaller mesh size leads to a smaller step time for explicit Eulerian methods, making the whole computation time much longer because the upper bond of step time is proportional to the mesh size. On the contrary, the computation time of POSS increases linearly with the number of nodes when linear interpolation is used. Furthermore, the step time required for POSS is almost independent with the mesh since the mesh size slightly affects the UBS condition. Thus, the step size (determining the number of unknowns) of POSS could be very small. In higher dimensions when a large number of unknowns are introduced, the most time-consuming part is the interpolation, which could be accelerated using parallel computation.

4.4 Extension to other coordinate systems

The extension of POSS to cylindrical and spherical coordinate systems is straightforward. The basic idea is to solve the position subproblem on Cartesian coordinate by replacing ‘ u ’ with ‘ ru ’ and ‘ r^2u ’, respectively. At the same time, the state subproblem is solved in the corresponding coordinate systems.

Let us take the 2D cylindrical coordinate system (r - z system) as an example. Re-write equation (2.3) in r - z system below

$$\frac{\partial ru}{\partial t} + \left(v_r \frac{\partial ru}{\partial r} + v_z \frac{\partial ru}{\partial z} \right) = 0 \quad (4.4)$$

where r and z denote the radial distance and height, respectively. In equation (4.4) the term ' ru ' can be viewed as the 'modified' unknown in Cartesian coordinate system. This value of u is obtained by mapping of ' ru ' from the auxiliary mesh to the reference mesh and then divided by r . The value on the symmetry axis should be taken care of since $r = 0$. To handle this, r is modified by adding a very small tolerance to avoid division by zero.

5 Numerical experiments

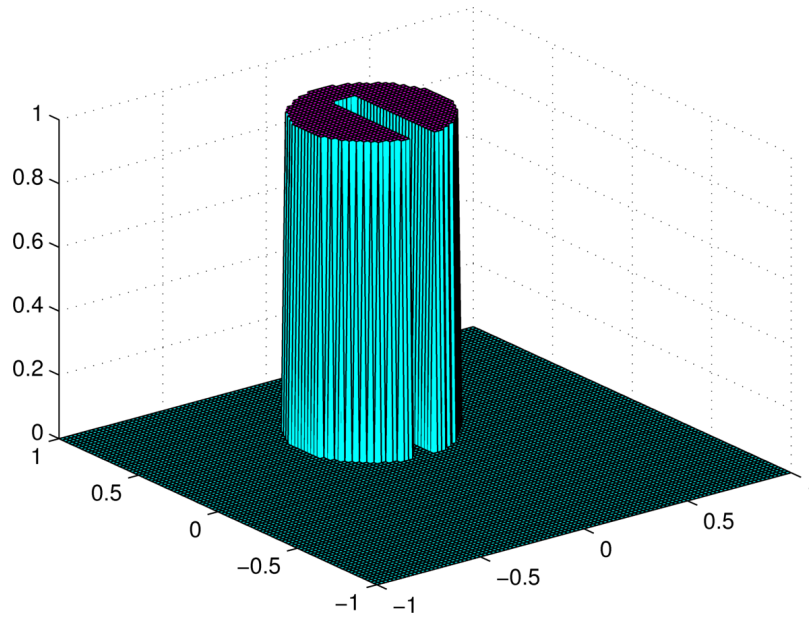
5.1 Rotation of a Cylinder with a slot

One of the most classical numerical tests is the rotation of a cylinder with a slot in a non-uniform velocity field $\mathbf{v} = (-y, x)$ [6, 10]. The cylinder will rotate counterclockwise around the center of the square domain $(-1, 1) \times (-1, 1)$. The initial profile of this cylinder is defined by

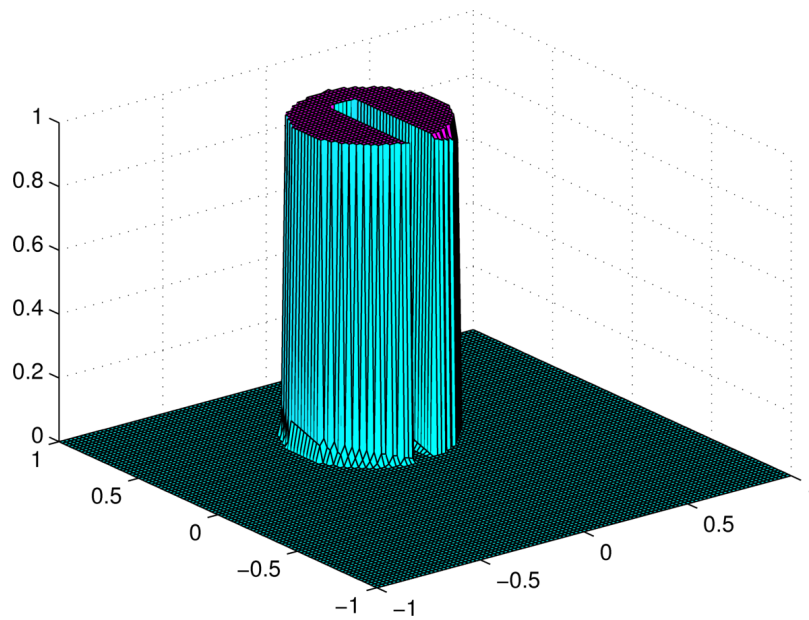
$$u_0(x, y) = \begin{cases} 1, & \text{if } R < \frac{1}{3} \text{ and } (|x| > 0.05 \text{ or } y > 0.5) \\ 0, & \text{otherwise} \end{cases} \quad (5.1)$$

where $R = \sqrt{x^2 + (y - \frac{1}{3})^2}$, as shown in Fig.5.1 (a).

It takes a period 2π time for the cylinder to come a full circle. Since the velocity field is not stiff, first order Euler method is used to solve the position subproblem. If $2 \times 100 \times 100$ uniform triangle elements are used, the step time of CFL condition is at least 0.01. However, the step time for POSS could be chosen as 0.1 or larger, which is 10 times larger than that of CFL condition. Moreover, during each step, only the position subproblem needs to be solved since the divergence of velocity is zero. Thus, extremely fast solution is obtained. Fig.5.1 illustrates the profile of cylinder after one period. It is clear that a very high resolution is achieved.



(a)



(b)

Fig.5.1. Simulation results (a) Initial condition ($t = 0$). (b) $t = 2\pi$. The step time is 0.1.

5.2 General advection-diffusion problem test

There exists analytical solutions for the 1D advection-diffusion equation even with variable coefficients [27], which enables us to compare it with the numerical solution. For example, let us consider the problem for $D = (1 - x)^2$, $v = 1 - x$ and $f = 0$ in equation (1.1) with the boundary condition

$$u(0, t) = 1, u(1, t) = 0 \quad (5.2)$$

the exact solution is

$$u(x, t) = \frac{1}{1-x} \operatorname{erfc} \left\{ \frac{\ln(1-x)}{-2\sqrt{t}} \right\} \quad (5.3)$$

where erfc is the complementary error function.

Note that in this case, the diffusion coefficient is not constant. Thus equation (2.3) turns into

$$\frac{\partial u}{\partial t} + \left(v - \frac{\partial D}{\partial x} \right) \frac{\partial u}{\partial x} = 0 \quad (5.4)$$

which is solved by first order Euler method. The equation (2.2) is solved by first order BDF (also called as backward Euler method). The calculations are performed for a space step 5×10^{-3} and a time step of 10^{-3} . Fig.5.2 shows the comparison between the analytic solution and the numerical results obtained with POSS for this case. As it can be seen, there is an excellent agreement between the curves, validating the POSS to solve the general advection-diffusion problems with changing diffusion coefficient.

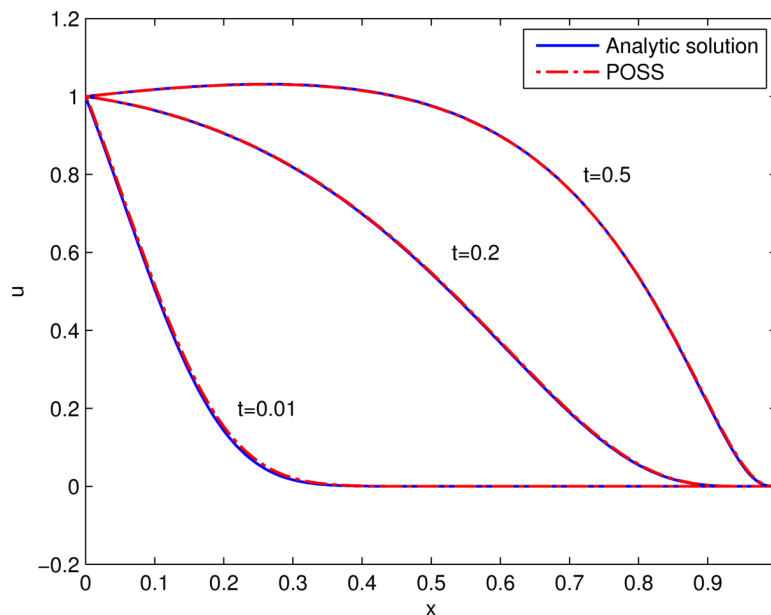


Fig.5.2. Comparison of analytic solution and numerical solution using POSS.

5.3 Davies test

5.3.1 1D Davies test

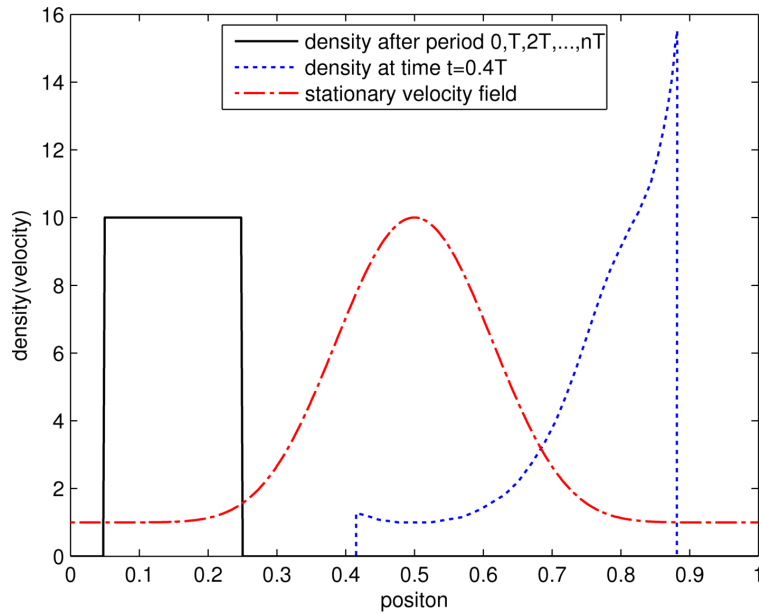
The Davies test was first introduced by Davies and Niessen [28] to test the performance of high-resolution algorithms for very stiff problems. This test consists of the transport of a square density profile through a stationary oscillating velocity field, as shown in Fig.5.3 (a). The equations below give the expression for the density and velocity, respectively.

$$u_0(x) = \begin{cases} 10, & \text{if } 0.05 \leq x \leq 0.25 \\ 0, & \text{otherwise} \end{cases} \quad (5.5)$$

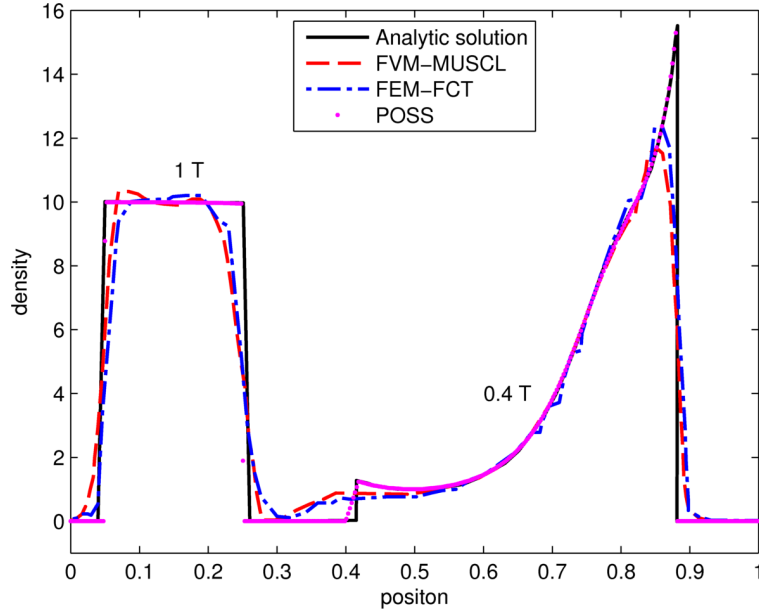
$$v(x) = 1 + 9\sin^8(\pi x) \quad (5.6)$$

which is governed by the equation (1.1) with $D = 0, f = 0$.

After one period $T \approx 0.591$, the square will return back to its original position. This problem was solved using POSS with 400 uniform cells. The time step is set to 2.4×10^{-3} s. Both the position equation and state equation are solved using third order TVD-RK method (the same as later tests in 2D and 3D). Fig.5.3 (b) shows a comparison of the solution at two different time instants calculated with the FVM-MUSCL, FEM-FCT and POSS. Observe the excellent agreement of the estimations with POSS and the analytic solution. The average of the absolute error after one period is equal to 0.2650 and 0.2677 for FVM-MUSCL and FEM-FCT algorithms, respectively [29]. This error is only 0.004 for POSS with the same mesh.



(a)



(b)

Fig.5.3. (a) Initial conditions for the density and the velocity field and exact solution after 0.4 period. (b) Density solution at times 0.4 T and T obtained from the FVM-MUSCL, FEM-FCT algorithms and POSS.

5.3.2 2D Davies test

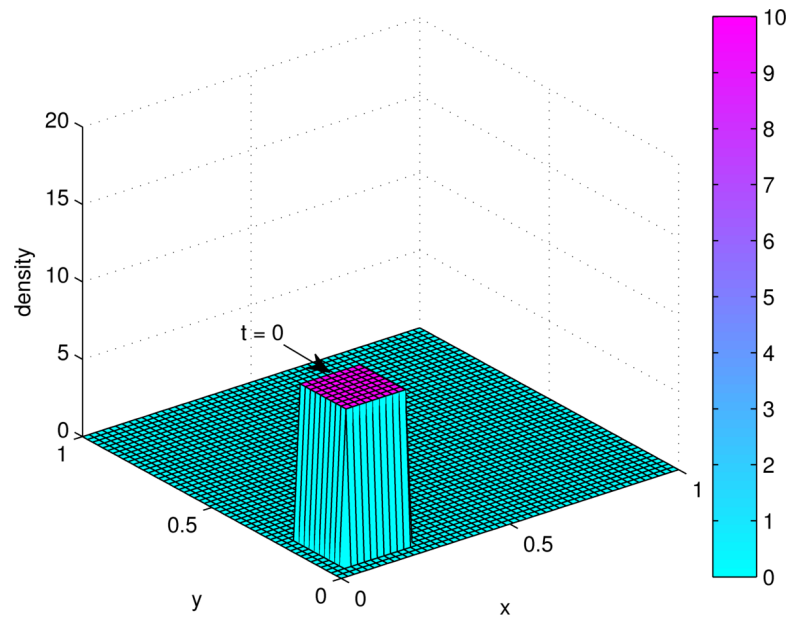
Davies test case can be easily extended to high dimensions. The initial condition is given by

$$u_0(j_1, j_2, \dots) = \begin{cases} 10, & \text{if } 0.05 \leq j_1, j_2, \dots \leq 0.25 \\ 0, & \text{otherwise} \end{cases} \quad (5.7)$$

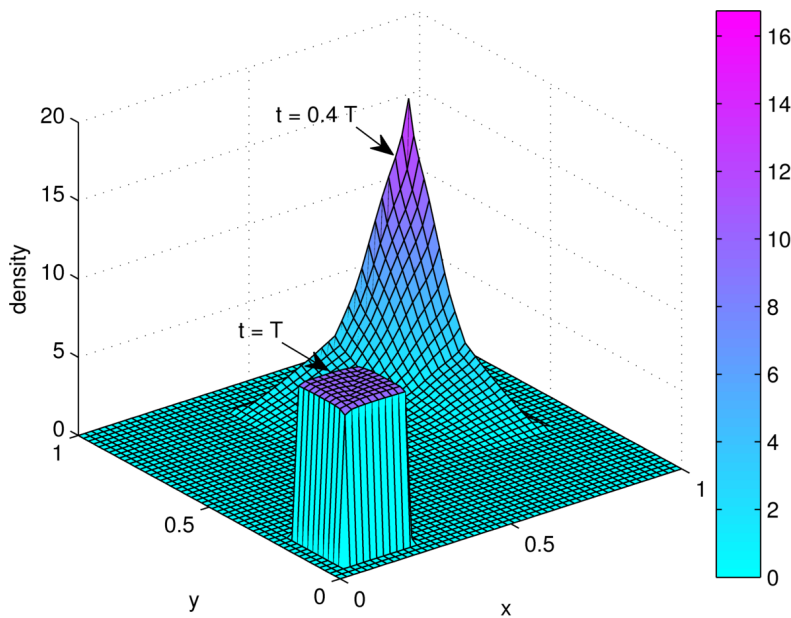
where j_1, j_2, \dots represent dimensions. The velocity is then defined by

$$v_j = 1 + 9\sin^8(\pi j), \quad j = j_1, j_2, \dots \quad (5.8)$$

The initial condition of Davies test in 2D is shown in Fig.5.4 (a). Fig.5.4 (b) illustrates the simulation results at $t = 0.4 T$ and T using POSS with $2 \times 50 \times 50$ triangle cells. The time step is 4.7×10^{-3} . Note the high resolution of the 2D solution obtained with POSS for this very stiff numerical problem.



(a)



(b)

Fig.5.4. Simulation results of POSS for Davies test in 2D (a) initial condition. (b) density distribution at $t = 0.4T$ and T .

To compare the simulation time for different meshes, the simulations are executed on meshes with 625, 2 500, 10 000, 40 000, 90 000 and 160 000 nodes, respectively. Fig.5.5 plots the normalized simulation time as a function of the number of unknowns. It is clear that the time complexity increases linearly with the number of unknowns. This is because the projection step

of the simulation dominates the execution time, which has linear complexity when linear interpolation is used.

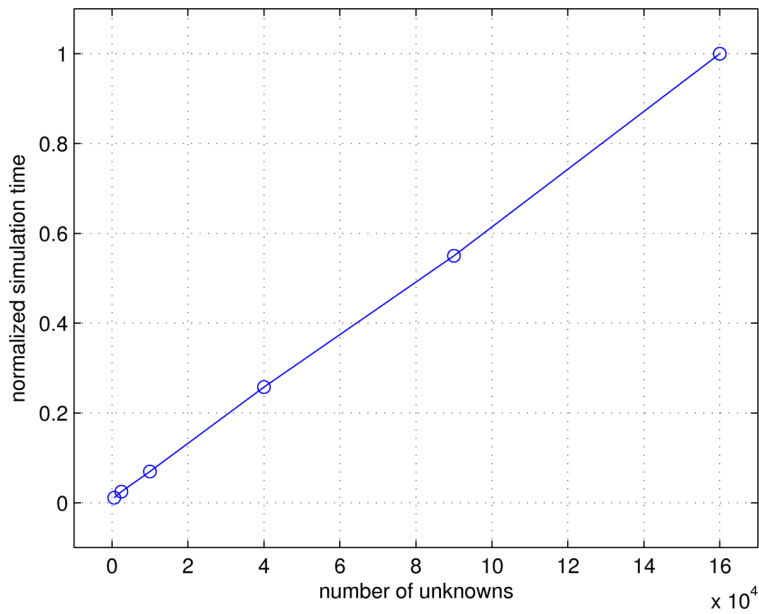
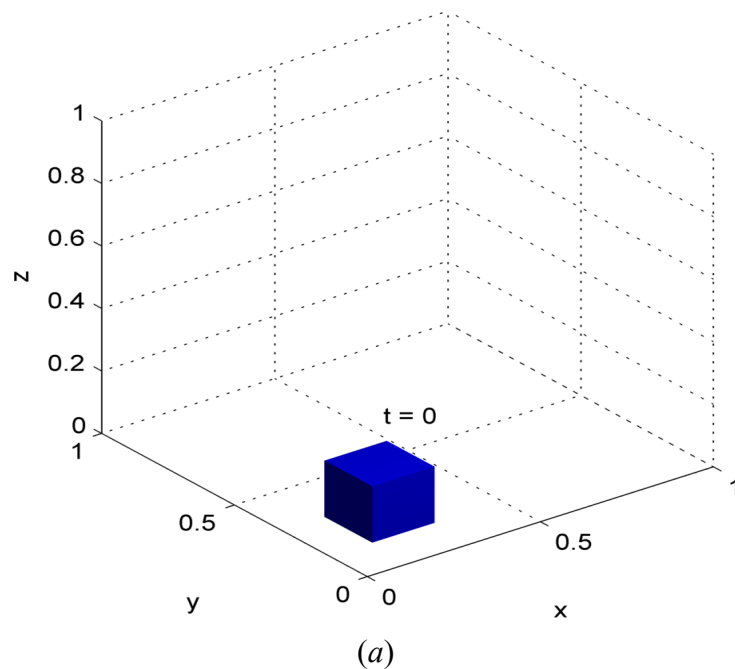


Fig.5.5. The simulation time as a function of the number of unknowns, normalized to the maximum execution time.

5.3.3 3D Davies test

In order to visualize the density distribution of Davies test in 3D, the isosurface where the density equals to 9.5 is plotted. The numerical simulation is performed with 192 000 tetrahedron elements. The time step is set as 4.7×10^{-3} s.



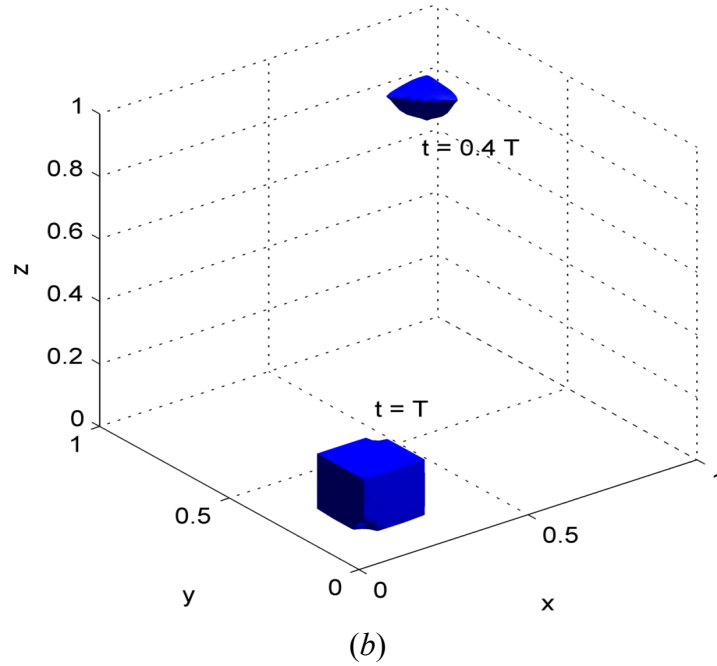


Fig.5.6. Simulation results of Davies test in 3D (a) initial condition. (b) density distribution at $t = 0.4T$ and T .

As can be seen from Fig.5.6 (b), the cubic isosurface returns back to its initial position after a period. Only very small diffusion around two corners is found. High resolution at other regions is obtained. The maximum relative error after one period is only 0.65%. The above Davies tests in three dimensions show that POSS could be easily extended to high dimensions.

5.4 2D streamer discharge test

In order to further validate POSS in complex 2D problems and in cylindrical coordinates, a two-dimensional streamer discharge model is tested. It considers an ellipsoid plasma spot (electron and positive ion seed) released at the center of the two parallel plates. Due to the high applied voltage, a double-headed streamer will be formed and propagate to the plates. The model, initial condition and parameters are the same as the 2D test reported in [30].

A non-uniform mesh is here used where very fine mesh size ($10 \mu m$) is applied around the axis of symmetry. This yields a mesh with about 200000 triangle elements. As in the previous 2D tests, both the position and state subproblems are solved using third order TVD-RK method.

Fig.5.7 illustrates the distribution of the strength of electric field in 0.5, 1.5 and 2.5 ns. Fig.5.8 shows the axial electric field profile compared with the results using the moving-mesh ULTIMATE QUICKEST scheme (hereinafter called MM-QUICKEST). Both Fig.5.7 and Fig.5.8 show an overall agreement of the results using POSS and MM-QUICKEST.

In this streamer test, the LBA condition is not satisfied where the velocity is low as previously discussed in Section?,. However, the numerical diffusion caused by interpolation in these regions affects little since the distribution of velocity and density of both electrons and positive ions are quiet smooth. Thus, POSS gives a high resolution results as shown in Fig.5.8.

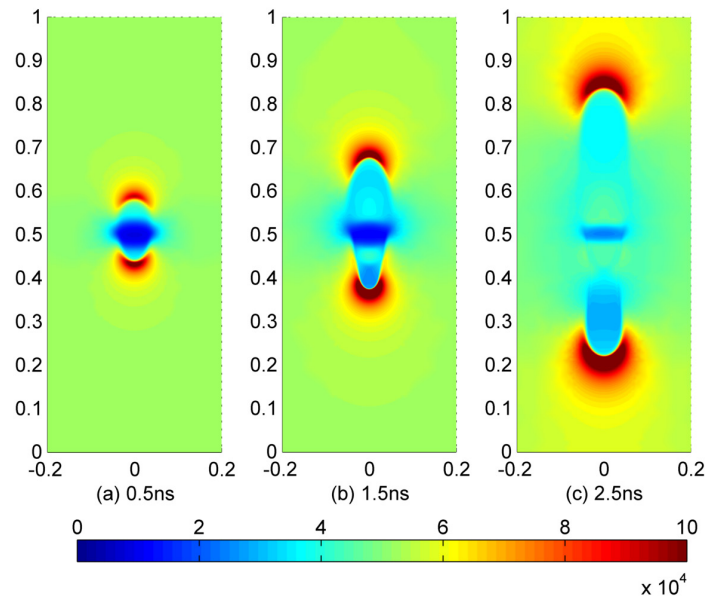


Fig.5.7. Simulation results of electric field distribution (unit in V/cm)

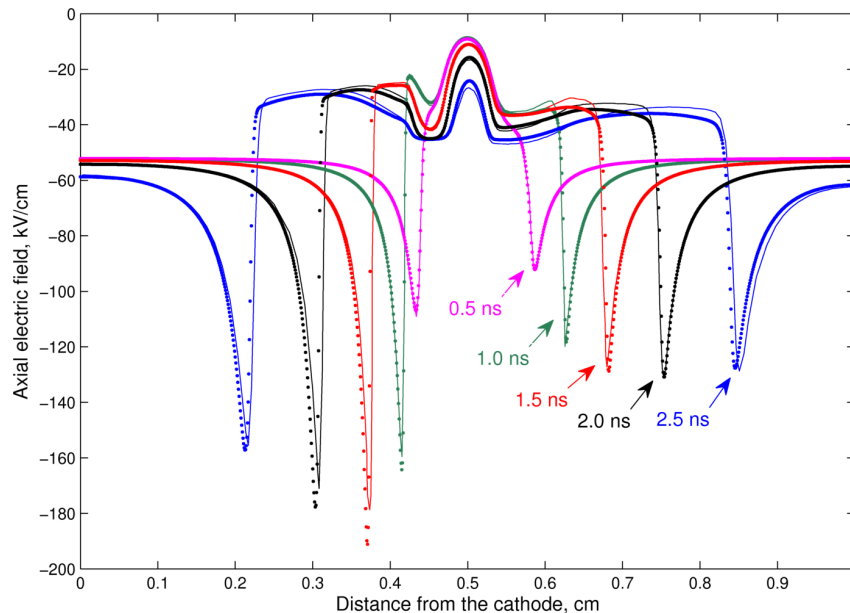


Fig.5.8. The axial electric field along the axis of symmetry at various time obtained by POSS and MM-QUICKEST [30].

To obtain high resolution for MM-QUICKEST, very fine mesh has to be used. This results in a very small time step. Moreover, the procedure of flux correction has to be applied during each

loop. These two points means long simulation time. Instead, the time step of POSS is not restricted to CFL condition and the only time-consuming part, the projection step can be speed up with parallel computation. This ensures that POSS is a very fast numerical method.

6 Conclusion

A simple, fast, oscillation-free, high-resolution algorithm for convection-dominated flows: the position-state separation method (POSS) is proposed. The stability, accuracy, time complexity and high order time discretization are discussed. Several numerical experiments are conducted to demonstrate the low computational cost, robustness, and high-resolution of the POSS. Several conclusions can be drawn

- 1) POSS is not restricted by CFL condition; the time complexity of POSS is linear to the unknowns when dealing with the convection-dominated flows.
- 2) POSS can be easily extended to cylindrical and other coordinate systems and also to high dimensions.
- 3) POSS combined with high order TVD-RK method can solve very stiff problems.
- 4) POSS is easy to be implemented and parallelized.

In addition, CDR equation is only one partial differential equation expressed in a conservation form. Since Navier-stokes equations can also be expressed in a conservation form, POSS can also solve them. The details of such application of POSS will be reported in the future publication.

Acknowledgments

L.L. greatly appreciates the scholarship support from China Scholarship Council (CSC). M.B would like to acknowledge the financial support of the Swedish strategic research program StandUp for Energy.

References

- [1] O. Shipilova, *et al.*, "Particle transport method for convection problems with reaction and diffusion," *International Journal for Numerical Methods in Fluids*, vol. 54, pp. 1215-1238, 2007.

- [2] A. Smolianski, *et al.*, "A fast high - resolution algorithm for linear convection problems: particle transport method," *International Journal for Numerical Methods in Engineering*, vol. 70, pp. 655-684, 2007.
- [3] J. P. Boris and D. L. Book, "Flux-corrected transport. I. SHASTA, A fluid transport algorithm that works," *Journal of Computational Physics*, vol. 11, pp. 38-69, 1973.
- [4] D. L. Book, *et al.*, "Flux-corrected transport II: Generalizations of the method," *Journal of Computational Physics*, vol. 18, pp. 248-283, 1975.
- [5] J. P. Boris and D. L. Book, "Flux-corrected transport. III. Minimal-error FCT algorithms," *Journal of Computational Physics*, vol. 20, pp. 397-431, 1976.
- [6] S. T. Zalesak, "Fully multidimensional flux-corrected transport algorithms for fluids," *Journal of Computational Physics*, vol. 31, pp. 335-362, 1979.
- [7] R. Morrow and L. Cram, "Flux-corrected transport and diffusion on a non-uniform mesh," *Journal of Computational Physics*, vol. 57, pp. 129-136, 1985.
- [8] R. Löhner, *et al.*, "Finite element flux-corrected transport (FEM-FCT) for the euler and Navier-Stokes equations," *International Journal for Numerical Methods in Fluids*, vol. 7, pp. 1093-1109, 1987.
- [9] R. Löhner, *et al.*, "A finite element solver for axisymmetric compressible flows," presented at the AIAA, Fluid Dynamics, 20th Plasma Dynamics and Lasers Conference, 1989.
- [10] D. Kuzmin and S. Turek, "Flux correction tools for finite elements," *Journal of Computational Physics*, vol. 175, pp. 525-558, 2002.
- [11] B. Van Leer, "Towards the ultimate conservative difference scheme. V. A second-order sequel to Godunov's method," *Journal of Computational Physics*, vol. 32, pp. 101-136, 1979.
- [12] B. P. Leonard, "A stable and accurate convective modelling procedure based on quadratic upstream interpolation," *Computer Methods in Applied Mechanics and Engineering*, vol. 19, pp. 59-98, 1979.
- [13] C.-W. Shu, "Total-variation-diminishing time discretizations," *SIAM Journal on Scientific and Statistical Computing*, vol. 9, pp. 1073-1084, 1988.
- [14] B. Cockburn, *et al.*, "TVB Runge-Kutta local projection discontinuous Galerkin finite element method for conservation laws III: one-dimensional systems," *Journal of Computational Physics*, vol. 84, pp. 90-113, 1989.
- [15] B. Cockburn and C.-W. Shu, "TVB Runge-Kutta local projection discontinuous Galerkin finite element method for conservation laws. II. General framework," *Mathematics of Computation*, vol. 52, pp. 411-435, 1989.
- [16] B. Cockburn, *et al.*, "The Runge-Kutta local projection discontinuous Galerkin finite element method for conservation laws. IV. The multidimensional case," *Mathematics of Computation*, vol. 54, pp. 545-581, 1990.
- [17] B. Cockburn and C.-W. Shu, "The Runge-Kutta discontinuous Galerkin method for conservation laws V: multidimensional systems," *Journal of Computational Physics*, vol. 141, pp. 199-224, 1998.
- [18] C. Johnson, "A new approach to algorithms for convection problems which are based on exact transport + projection," *Computer Methods in Applied Mechanics and Engineering*, vol. 100, pp. 45-62, 1992.

- [19] O. Pironneau, *Finite element methods for fluids*: Wiley Chichester, 1989.
- [20] O. Pironneau, *et al.*, "Characteristic-Galerkin and Galerkin/least-squares space-time formulations for the advection-diffusion equation with time-dependent domains," *Computer Methods in Applied Mechanics and Engineering*, vol. 100, pp. 117-141, 1992.
- [21] O. Chanrion and T. Neubert, "A PIC-MCC code for simulation of streamer propagation in air," *Journal of Computational Physics*, vol. 227, pp. 7222-7245, 2008.
- [22] H. Okuda, "Nonphysical noises and instabilities in plasma simulation due to a spatial grid," *Journal of Computational Physics*, vol. 10, pp. 475-486, 1972.
- [23] G. I. Marchuk, "Splitting and alternating direction methods," in *Handbook of Numerical Analysis*. vol. Volume 1, P. G. Ciarlet and J. L. Lions, Eds.: Elsevier, 1990, pp. 197-462.
- [24] J. Albery, *et al.*, "Remarks around 50 lines of Matlab: short finite element implementation," *Numerical Algorithms*, vol. 20, pp. 117-137, 1999.
- [25] D. S. Kershaw, "The incomplete Cholesky—conjugate gradient method for the iterative solution of systems of linear equations," *Journal of Computational Physics*, vol. 26, pp. 43-65, 1978.
- [26] S. Gottlieb and C.-W. Shu, "Total variation diminishing Runge-Kutta schemes," *Mathematics of Computation of the American Mathematical Society*, vol. 67, pp. 73-85, 1998.
- [27] A. Kumar, *et al.*, "Analytical solutions to one-dimensional advection–diffusion equation with variable coefficients in semi-infinite media," *Journal of Hydrology*, vol. 380, pp. 330-337, 2010.
- [28] A. Davies and W. Niessen, "The solution of the continuity equations in ionization and plasma growth," in *Physics and Applications of Pseudosparks*: Springer, 1990, pp. 197-217.
- [29] O. Ducasse, *et al.*, "Critical analysis on two-dimensional point-to-plane streamer simulations using the finite element and finite volume methods," *Plasma Science, IEEE Transactions on*, vol. 35, pp. 1287-1300, 2007.
- [30] D. Bessières, *et al.*, "A new one-dimensional moving mesh method applied to the simulation of streamer discharges," *Journal of Physics D: Applied Physics*, vol. 40, pp. 6559-6570, 2007.